

# THE 4TH INTERNATIONAL CONFERENCE ON ALUMINUM ALLOYS

## PROCESS MAPS FOR ALUMINIUM - LITHIUM ALLOYS

Amol A. Gokhale<sup>1</sup>, Vijaya Singh<sup>1</sup>, N. Eswara Prasad<sup>1</sup>, C.R. Chakravorty<sup>1</sup>  
and Y.V.R.K. Prasad<sup>2</sup>

1. Defence Metallurgical Research Laboratory, Kanchanbagh, Hyderabad 500258, INDIA

2. Department of Metallurgy, Indian Institute of Science, Bangalore 560 012, INDIA

### Abstract

The intrinsic workability of near- 8090 Al-Li alloys was evaluated and represented in the form of 'process stability' and 'process efficiency' maps over the temperature range 300-550 °C and strain rate range  $10^{-3}$  -  $10^2$  s<sup>-1</sup>. The process stability parameter became increasingly negative with decreasing temperature and increasing strain rate, while the process efficiency parameter increased with increasing temperature and decreasing strain rate. Microstructural evaluation confirmed the existence of localised flow in cases where the stability parameters were either low or negative. Dynamically recrystallised microstructures resulted when process efficiencies were in the range 0.3 to 0.4. Trace additions of Be and lowering of Li content shifted the contours towards greater process stability and higher efficiencies, and resulted in improvements in tensile and notch tensile properties.

### Introduction

The overall workability of a material is composed of two parts: (i) intrinsic workability and (ii) state-of-stress workability. The intrinsic workability of a material, which is related to its constitutive behaviour, depends upon the chemical composition, microstructure and processing history, and its response to the applied temperature, strain rate and extent of strain in processing. On the other hand, the state-of-stress workability depends upon the geometry of the deformation zone and the applied stress state in a mechanical process. Both the workabilities must be taken into consideration when optimising a deformation route for processing of wrought alloys. Among the two workabilities, the former, evaluated here, is independent of the type of deformation process employed, such as rolling, forging, extrusion etc, and therefore, has wider applicability. One of the commonly used maps which represent the intrinsic workability of a material are known as 'Raj' maps [1]. These maps show the regimes of temperature-strain rate space, where different deformation and fracture mechanisms are operative and, in many cases, they also delineate 'safe' processing regimes.

In the present approach, the work piece is considered as a dissipater of power in the total metal working system. The total power absorbed by the work piece at any instant is dissipated by (a) plastic work, most of which is converted into heat (the G content) and (b) dynamic metallurgical processes (the J co-content) such as dynamic recovery (DR), dynamic recrystallisation (DRX), internal fracture, formation and/or dissolution of precipitates, phase transformation etc. occurring during hot working.

It is desirable that the work piece dissipates the highest possible power through dynamic metallurgical processes (i.e. maximization of  $J$ ). One such parameter, which represents the power dissipation ability of a material can be expressed in terms of the efficiency of dissipation,  $\eta$ , which is defined as the ratio of  $J$  to  $J_{\max}$ . It can be shown [2] that

$$\eta = J/J_{\max} = 2m/(m+1) \quad (1)$$

where  $m$  is the strain rate sensitivity of the alloy, calculated from the constitutive relations of the material of the type  $\sigma = \sigma(T, \dot{\epsilon}, \epsilon)$  obtained from, say, hot compression tests.

It has been further shown [3] that flow instability (which may manifest as adiabatic shear bands, localised shear bands, Luders bands, flow rotations etc) will occur during hot deformation if

$$\xi(\dot{\epsilon}) = \frac{d \ln(m / m + 1)}{d \ln \dot{\epsilon}} + m < 0 \quad (2)$$

where  $\xi(\dot{\epsilon})$  is termed as the stability parameter. The variations of the process efficiency parameter ( $\eta$ ) and the process stability parameter ( $\xi$ ) with temperature and strain rate, presented as equi-parameter contours over a  $T$ - $\dot{\epsilon}$  space are known as the 'process efficiency' and 'process stability' maps. The stability maps delineate 'safe' from 'unsafe' regions of hot working, while the efficiency maps provide the exact temperature - strain rate combination which is associated with given values of the process efficiency parameter which, in turn, can be correlated with certain dynamic metallurgical processes. For processing of materials, the most favourable conditions are those which provide highest  $J$  dissipated in the most efficient fashion (highest  $\eta$ ), and lie outside the regions where flow instabilities are expected. This method has been successfully applied for the optimisation of various engineering materials including zirconium, nickel, a metal matrix composite and a Mg-alloy ZM21 [3,4].

In the present work, the process maps have been established for identifying the suitable hot working parameters, and also to compare the intrinsic workabilities of Al-Li alloys of different compositions. The mechanical properties of these alloys extruded to rod forms are evaluated, and the results are presented.

### Experimental

Aluminium -lithium alloys were prepared by air induction melting under flux cover and then cast in chill moulds under argon cover. The chemical compositions of the four alloys are given in Table I. Cylindrical ingots were homogenised at 535 °C for 40 hrs and machined to 50 mm dia for extrusion. Specimens for hot compression tests (10 mm dia. x 15 mm long) were machined from the sliced portions of the extrusion billet. Remaining portions of the billets were extruded at 540 °C with an area reduction of 17.5:1 at an average strain rate of 0.2 s<sup>-1</sup>.

Hot compression tests were carried out on a Dartec system at constant temperatures in the range of 300 - 550 °C and at constant true strain rates over the range 10<sup>-3</sup> - 10<sup>2</sup> s<sup>-1</sup>. True stress - true strain data were stored during each test from which the strain rate sensitivity parameter 'm' was calculated for different temperatures and strain rates. Process stability and efficiency parameters were calculated from relations (1) and (2) given above and plotted as isoparameter contours over the temperature - strain rate domain studied.

Table I. Chemical Composition of the Alloys Prepared (wt. %), Balance Aluminium

Alloy Code	Li	Cu	Mg	Zr	Be	Fe	Si
A	2.12	1.10	0.87	0.09	0.026	0.08	0.04
B	2.32	1.18	0.92	0.08	0.033	0.08	0.04
C	1.85	1.15	0.91	0.09	----	0.07	0.04
D	2.32	1.18	0.97	0.07	----	0.08	0.04

Microstructures in the as-cast, homogenised, hot compressed and extruded conditions were studied by optical microscopy. Extruded rods were heat treated to T6 temper (535 °C /45 min - water quench - 190 °C /24h). Tensile properties were determined on ASTM E8M specified round specimens with 25 mm gauge length. Notch tensile strength was determined in the heat treated condition from the samples prepared as per ASTM standard E602 . The ratio of notch tensile strength to yield strength was evaluated.

### Results and Discussion

The typical as- cast and homogenised microstructures are shown in Figure 1. The as- cast microstructure is equiaxed dendritic, with the grain size of about 200-250  $\mu\text{m}$  and secondary dendrite arm spacing of about 60  $\mu\text{m}$ , which are typical of TiAlB1 inoculated Al-Li alloys solidified at an average cooling rate of 0.5 °C/s [5]. Homogenisation removes most of the segregation products; however, intermetallic particles containing Fe and Si remain undissolved.

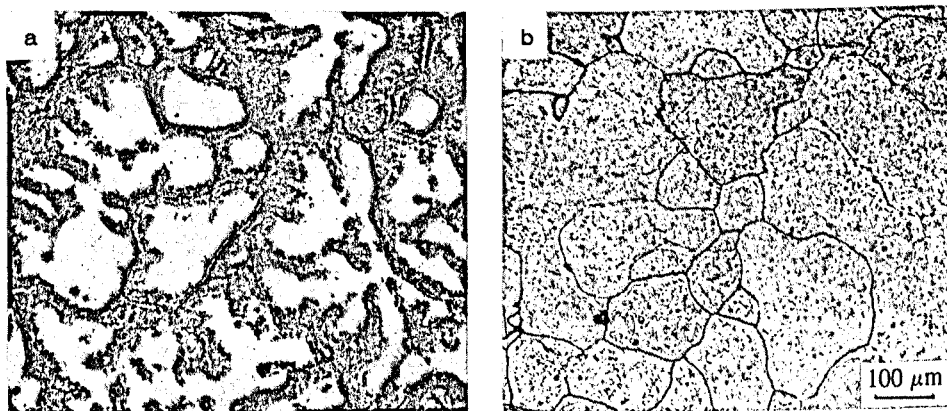


Figure 1. Alloy 'A' microstructures in the (a) as cast and (b) homogenised conditions.

Typical true stress - true strain curves obtained for alloy A at 500 °C at different strain rates are shown in Figure 2. The nature of the curves remained similar over the entire range of temperatures studied for all the alloys. The true stress was found to reach steady state

values at a total strain of 0.4 or less in all cases except at very high strain rates. At very high strain rates ( $100 \text{ s}^{-1}$  and in some cases  $10 \text{ s}^{-1}$ ) flow softening was observed. The values of maximum as well as the steady state true stress increase with decreasing temperature (not shown here) and increasing strain rate, as expected.

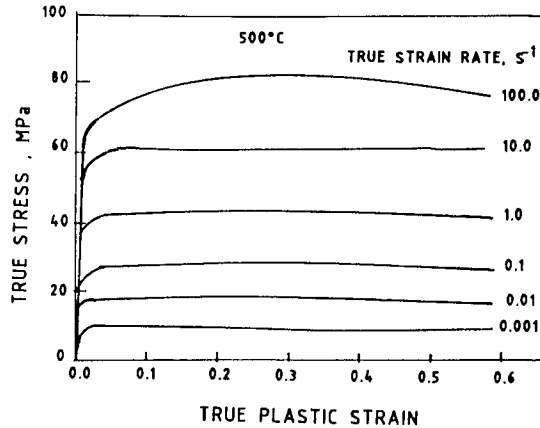


Figure 2. True stress Vs. true strain data obtained at  $500^\circ\text{C}$  and for different strain rates for alloy A

Typical process stability and efficiency maps (for alloy A) are shown in Figures 3 and 4, respectively. Values of the stability and efficiency parameters are shown to increase with increasing temperature and decreasing strain rate. Steep increase in the efficiency parameter with decreasing strain rates at high temperatures (which indicates wedge cracking) or rapid increase in efficiency with falling temperatures at high strain rates (indicating void formation) were not observed.

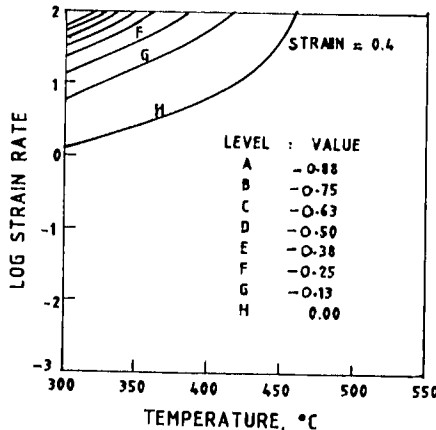


Figure 3. Process stability map for alloy A. Stability parameters corresponding to each contour are shown. The flow is unstable within the regime bounded by contour H where  $\xi(\dot{\epsilon})$  is negative.

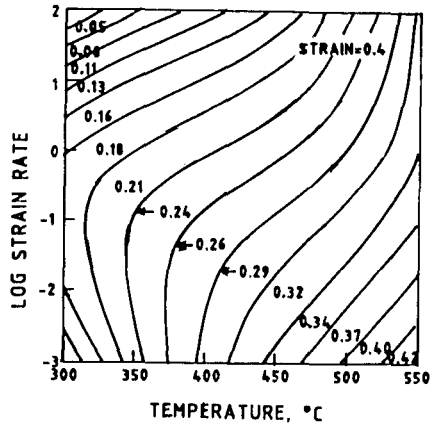


Figure 4. Process efficiency map for alloy A. Efficiency parameters corresponding to each contour are shown.

Figure 5 shows the microstructures obtained from the axial sections of the hot compression test specimens deformed under conditions corresponding to the four corners of the maps shown in Figures 3 and 4, and an intermediate T- $\dot{\epsilon}$  combination. Specimens deformed at 300 °C show an unrecrystallised grain structure with banding which is indicative of localised flow (Fig 5 a, b). No void formation was observed in such cases. The corresponding deformation conditions represented low or negative stability parameters and very low efficiency parameters (0.05 for  $10^2 \text{ s}^{-1}$  and 0.13 for  $10^{-3} \text{ s}^{-1}$ ). The microstructure became highly recrystallised when deformation was carried out at the highest temperature employed, i.e. at 550 °C (Fig 5 d, e). The degree of recrystallisation increased when the strain rate decreased from  $10^2 \text{ s}^{-1}$  to  $10^{-3} \text{ s}^{-1}$  (corresponding to an increase in the efficiency parameter from 0.32 to 0.42). At an intermediate temperature-strain rate combination (having  $\eta = 0.29$ ), recrystallisation was only partial and appeared to have begun at grain boundary triple junctions in select areas (Fig 5 c). No wedge cracking was observed at the grain boundaries in the specimens deformed at 500-550 °C, indicating amenability for superplastic deformation. Thus lower strain rates and higher deformation temperatures are conducive to stable deformation and recrystallisation, which are accompanied by increase in the stability as well as the efficiency parameters.

The microstructure of the as-extruded rods is shown in Figure 6. About 75% of the outer cross section showed fully recrystallised microstructure (Figure 6 a), while the core remained partially recrystallised (Figure 6 b). These observations match well with map findings which predict high degree of recrystallisation for the deformation conditions used in the extrusion experiments. The variation in the microstructure of the core and the peripheral regions is considered to be due to the variations in the state of stress at these locations.

The second half of the paper describes the effect of alloy composition on the process maps and the properties. It was observed that the basic nature of the maps and microstructures remained similar for all the compositions studied. However, shifts in the regimes of stability and efficiency were observed with changing alloy composition. Figure 7 compares the zero-stability parameter contours, and Table II gives the maximum process efficiency parameters for all the four alloys studied. It is seen that the presence of Be and lowering of the Li content led to expansion of the regimes of stable deformation and also increase in the value of maximum efficiency. Although the mechanisms responsible for this behaviour are

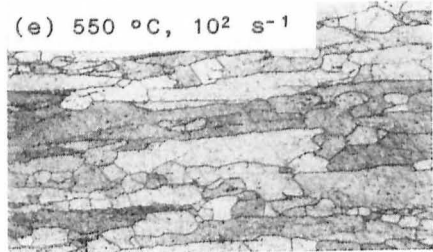
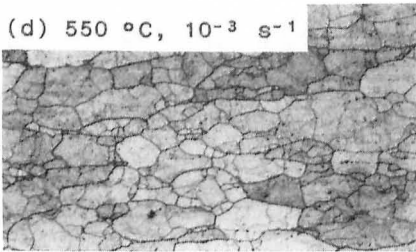
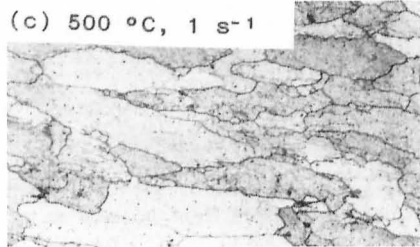
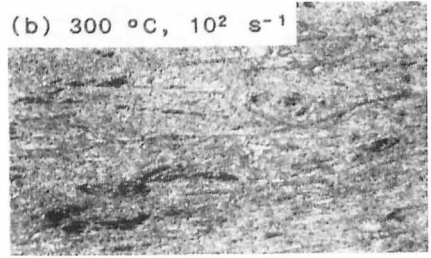
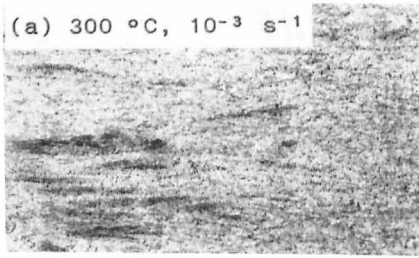


Figure 5. Microstructures of hot compression specimens deformed under different temperature (T) - strain rate ( $\dot{\epsilon}$ ) conditions.

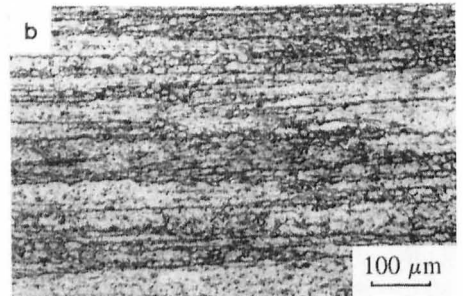
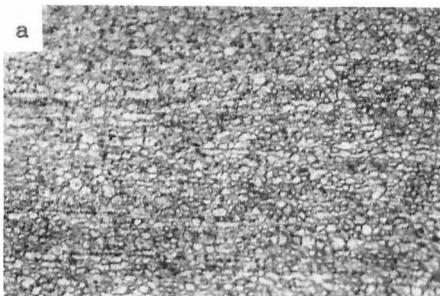


Figure 6. Microstructure of the as-extruded alloy A. (a) fully recrystallised outer region (b) partially recrystallised core region.

not fully understood, they are possibly related to the improved grain boundary mobility due to lower Li segregation at the grain boundaries.

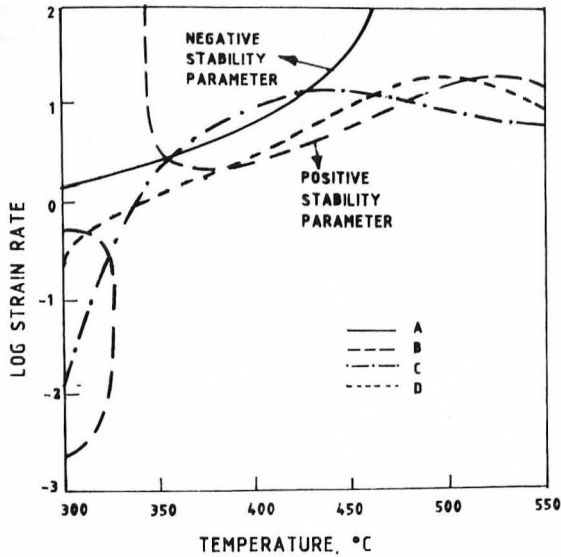


Figure 7. Comparison of the 'stable' processing zones for different alloys. Only the boundary contours for instability are shown for each of these alloys.

The tensile and notch tensile properties are reported in Table II. The ratio of the notch tensile strength to yield strength has previously been used as a measure of toughness [6]. The best combination of properties is found in the low-Li Be-containing alloy, which also exhibited high stability and efficiency of deformation. A comparison of the tensile fractographs for two alloys A (with low Li and trace Be) and D (with high Li and no Be), (see Fig. 7) showed that the fracture path consisted of both grain boundary and transgranular shear components. The shear component appeared to be dominating in alloy A which again is an indication of higher toughness. The process maps can thus serve as a very important tool for alloy development.

Table II. Comparison of the maximum process efficiency parameter and mechanical properties of the different alloys (properties correspond to L direction).

Alloy Code	Max $\eta$	0.2%PS (MPa)	UTS (MPa)	Elong. (%)	Notch Strength Ratio: $\sigma(\text{NTS})/\sigma(\text{TYS})$
A	0.42	412	498	9.8	1.51
B	0.39	404	486	8.5	1.27
C	0.37	345	439	9.4	1.55
D	0.33	396	462	8.0	1.26

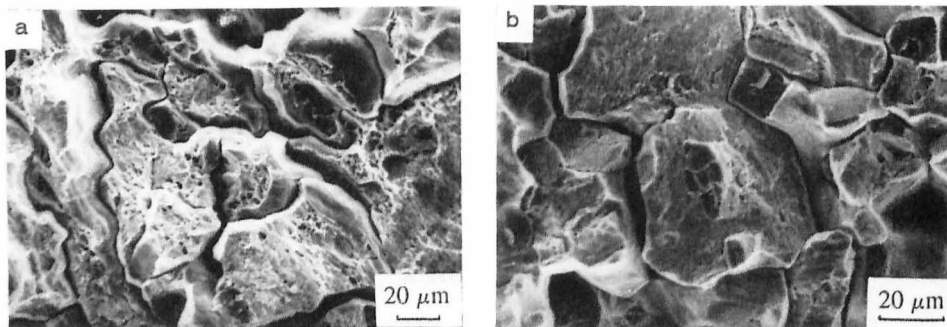


Figure 8. Tensile fractographs for extruded alloys. (a) alloy A (b) alloy D.

#### Conclusions

1. Process stability and efficiency maps were evaluated for a series of Al-Li alloys of different compositions.
2. A gradual increase in the stability and efficiency parameters with increasing temperature and decreasing strain rates was observed.
3. Higher temperatures and lower strain rates of deformation were associated with stable deformation (i.e. absence of flow localization) and increased extent of recrystallisation.
4. Decreasing Li content and trace additions of Be enlarged domains of stable deformation and increased the maximum efficiency. Also, the tensile and notch tensile property combinations have improved.

#### Acknowledgments

The authors wish to express their gratitude to Dr. P. Rama Rao, Secretary, DST, Govt. of India for his keen interest and support. We are grateful to our colleagues from DMRL and IISc for their invaluable help. Sincere thanks are also due to Mr SLN Acharyulu, Director, DMRL for the permission to publish this work.

#### References

1. R. Raj, Metall. Trans. **12A**, (1981), 1089.
2. Y.V.R.K. Prasad et al, Metall. Trans. **15A**, (1984), 1883.
3. Y.V.R.K. Prasad, Indian J. Technol. **28**, (1990), 435.
4. O. Sivakesavam, I.S. Rao and Y.V.R.K. Prasad, Mater. Sci. Technol. **9**, (1993), 805.
5. S. Sriram et al, Metastable Microstructures, Eds. D. Banerjee and L.A. Jacobson (New Delhi, INDIA: Oxford & IBH, 1993), 103.
6. P.J. Gregson and H.M. Flower, Acta Metall. **33(3)**, (1985), 527.